Analysis of the typical unified lattice Boltzmann models and a comprehensive multiphase model for convection-diffusion problems in multiphase systems

J. H. Lu, H. Y. Lei, and C. S. Dai*

Key Laboratory of Efficient Utilization of Low and Medium Grade Energy, MOE, Tianjin University, School of Mechanical Engineering, Tianjin University, 135 Yaguan Road, Jinnan District, Tianjin 300050, China

(Received 3 March 2019; revised manuscript received 30 May 2019; published 22 July 2019)

The present paper analyzes the typical unified lattice Boltzmann (LB) models for different convection-diffusion (CD) problems in multiphase systems. The CD problems in multiphase systems can be roughly classified into three groups: CD problems with a continuous scalar value and a continuous flux, a discontinuous scalar value and a continuous flux, a continuous scalar value and a discontinuous flux. The characteristics of the corresponding unified LB models for the three kinds of CD problems are analyzed and the equivalence between the LB models based on different perspectives or numerical schemes is revealed. Finally, a comprehensive multiphase LB model (CMLBM) capable of solving different isotropic and anisotropic CD problems in multiphase systems is proposed. Four typical CD problems in multiphase systems are calculated to validate the CMLBM; the results show that it performs well against the typical isotropic and anisotropic CD problems in multiphase systems.

DOI: 10.1103/PhysRevE.100.013307

I. INTRODUCTION

The lattice Boltzmann method (LBM) is based on the Boltzmann equation for describing the nonequilibrium process in statistical mechanics. It has been proven to be an efficient numerical method for simulating the nonequilibrium physical processes, such as fluid flows and different convection-diffusion (CD) problems. Furthermore, some developed lattice Boltzmann (LB) models have been proposed to simulate different CD problems in multiphase systems.

The different CD problems, e.g., heat transfer and mass transfer, in multiphase systems have similar governing equations which consist of the transient term, convection term, and diffusion term. According to the natural interface conditions, the CD problems in multiphase systems can be classified into three major groups: CD problems with a continuous scalar value and a continuous flux, a discontinuous scalar value and a continuous flux, a continuous scalar value and a discontinuous flux.

For the CD problems with a continuous scalar value and a continuous flux, heat transfer in multiphase systems can be considered as the typical example. The LB models to simulate heat transfer in the multiphase systems can be classified into two major groups: the discrete schemes and unified schemes. The discrete schemes solve the governing equation in different phases separately and need additional treatment for the phase interface to ensure the interface conditions. In this category, some difference methods [1–4] and interface treatments [5–7] have been proposed to treat the interface conditions. These discrete schemes share the same characteristics including extra effort to capture the interface position and complex calculation steps. These limitations prevent the discrete schemes from being prevalent to simulate practical problems with complex or moving interfaces.

The unified schemes, however, can solve the governing equations in different phases directly. Some research [8–11] has constructed the unified schemes by adding an additional term to the LB equation to correct the influence caused by different heat capacities of different phases. However, these methods need extra efforts to calculate the source term and bring some numerical errors to the results. One popular approach for constructing a unified model is modifying the equilibrium distribution function (EDF) [12–15]. The Chapman-Enskog expansion shows that the governing equation for heat transfer in multiphase systems can be recovered by using the modified EDF. In addition, the virtual heat capacity correction method [16] was applied to construct the unified LB model by modifying the physical model. The improved virtual heat capacity correction method [17] shows that the modifications of the physical model are equivalent to the modifications of the EDF. Another approach [18] is adjusting the model parameters to satisfy the interface conditions. The asymptotic analysis shows that the model can ensure the interface conditions with second-order accuracy.

In the CD problems with a discontinuous scalar value and a continuous flux, the conjugate mass transfer in multiphase systems can be considered as the typical case. Here the discussed LB models are based on the double film theory [19]. This problem is characterized by a concentration jump at the phase interface described by the double film theory, which brings additional difficulties to the simulations using the LB model. In the category of discrete schemes, Molaeimanesh and Akbari [20] proposed an interface treatment scheme to model the oxygen transfer across the gas-electrolyte interface in a cathode catalyst layer of a proton exchange membrane fuel cell. It shares the same characteristics of those discrete

Corresponding author: csdai@tju.edu.cn

schemes of conjugate heat transfer problems in multiphase systems.

In the category of unified schemes, Lu *et al.* [19] analyzed the physical mechanism of Henry's law and showed that Henry's law can be expressed as a relation between two weight coefficients in an EDF. By adjusting the weight coefficients, a unified LB model can be constructed. In another of their works [21], they analyzed the shortcomings of Fick's law in describing mass transfer in multiphase systems and then proposed a revised description of Fick's law. The governing equation based on the revised description of Fick's law has a similar expression with the governing equation of heat transfer in multiphase systems, and then a unified LB model can be constructed by modifying the EDF.

In the CD problems with a continuous scalar value and a discontinuous flux, the solid-liquid phase change can be considered as the typical case. The problem is characterized by the latent heat that keeps the interface temperature constant and the discontinuous heat flux at the phase interface. Most of the previous LB models for solving solid-liquid phase change problems are the unified schemes, since it is hard for the discrete schemes to deal with the discontinuous heat flux at a moving phase interface. Many LB models [22–30] consider the latent heat as an extra source term, which significantly increases the computation cost since the latent heat is implicit and has to be updated through iteration. On the other hand, by adding the latent heat into the total enthalpy, Huang *et al.* [31] proposed a new total enthalpy-based LB model. Thus the implicit latent enthalpy term can be eliminated, and then the iteration steps can be eliminated as well. Especially, Huang and Wu [32] proposed a multi-relaxation-time (MRT) LBE that can recover the standard governing equation with different heat capacities in the solid and liquid phases. Furthermore, they analyzed the appearance of the unphysical numerical diffusion resulting from the discontinuous heat flux at the phase interface and theoretically proved that the unphysical numerical diffusion of the one-dimensional one-phase melting problem can be eliminated by adjusting the relaxation parameters of the MRT model. Following their work, some researchers [33,34] extended the two-dimensional MRT model to three dimensions. In addition, Lu *et al.* [35] proposed an optimal two-relaxation-time (OTRT) LB model which can eliminate the unphysical numerical diffusion of an arbitrary D*m*Q*n* (*m* dimensions and *n* discrete velocities) LB model for both one-phase and two-phase melting problems.

In addition to the proposed LB models that focus on specific CD problems in multiphase systems, some researches focus on general CD problems in multiphase systems. On the one hand, some researchers proposed the general difference schemes [36–39] to treat different interface conditions, which can be considered as discrete schemes. Guo *et al.* [37] proposed an interface treatment for specified jumps of scale value and/or flux at the interface. Mu *et al.* [36] proposed a general interfacial treatment for continuous or discontinuous scalar value and flux. The scheme contains more interface condition types. Based on the boundary schemes [38] for Robin boundary conditions on straight or curved boundaries, Hu *et al.* [39] proposed an interfacial scheme for CD problems with general interfacial conditions, including conjugate conditions with or without jumps in heat and mass transfer, continuity of macroscopic variables and normal fluxes in ion diffusion in porous media with different porosity, and the Kapitza resistance in heat transfer.

On the other hand, some models [40,41] are based on the modified EDF, which can be considered as unified schemes. Even though the Chapman-Enskog expansion can recover the governing equation of the general CD problems, the expansion is based on continuous distribution functions by default, which means that the scalar value and flux should be continuous. Therefore, for the problem with a discontinuous scalar value or flux, special treatments are needed.

Compared with the discrete schemes, the unified schemes are easier in implementation and dealing with the complex and moving interfaces, which makes the unified schemes more attractive. Therefore, the present paper focuses on analyzing the typical unified LB models for CD problems in multiphase systems. The characteristics of the typical unified LB models for the three kinds of CD problems are respectively analyzed. The detailed mathematical analyses prove the equivalence between different LB models. Finally, the CMLBM, which considers the three kinds of isotropic and anisotropic CD problems in multiphase systems, is constructed. Several typical CD problems are calculated to validate the CMLBM, and the results show that CMLBM performs well in all the tests.

II. ANALYSIS OF THE TYPICAL UNIFIED LB MODELS

A. The MRT LB model for CD problems in a single phase

The general MRT lattice Boltzmann equation for CD problems can be expressed as

$$g_i(\mathbf{x}+\mathbf{e}_i\Delta t, t+\Delta t) = g_i(\mathbf{x},t) - [\mathbf{M}^{-1}\mathbf{S}\mathbf{M}]_{ij}\left[g_j(\mathbf{x},t) - g_j^{\mathrm{eq}}(\mathbf{x},t)\right], \quad (1)$$

where g_i is the discrete distribution function, g_i^{eq} is the EDF, $\mathbf{e}_i$ is the discretized velocity, $\mathbf{M}$ is the matrix that projects a vector onto the moment space $\mathbf{m}$, $\mathbf{S}$ is the relaxation matrix, and Δt is the time interval. In the present paper, the three-dimensional model with seven discrete velocities (D3Q7 model) is adopted for all the following discussions and simulations. The discrete velocities can be expressed as

$$[\mathbf{e}_0, \mathbf{e}_1, \mathbf{e}_2, \mathbf{e}_3, \mathbf{e}_4, \mathbf{e}_5, \mathbf{e}_6] = \begin{bmatrix} 0 & 1 & -1 & 0 & 0 & 0 & 0 \\ 0 & 0 & 0 & 1 & -1 & 0 & 0 \\ 0 & 0 & 0 & 0 & 0 & 1 & -1 \end{bmatrix} c, \quad (2)$$

where c is the lattice speed defined as $c = \Delta x/\Delta t = 1$ and Δx is the mesh interval. The matrix $\mathbf{M}$ is expressed as [42]

$$\mathbf{M} = \begin{bmatrix} 1 & 1 & 1 & 1 & 1 & 1 & 1 \\ 0 & 1 & -1 & 0 & 0 & 0 & 0 \\ 0 & 0 & 0 & 1 & -1 & 0 & 0 \\ 0 & 0 & 0 & 0 & 0 & 1 & -1 \\ 6 & -1 & -1 & -1 & -1 & -1 & -1 \\ 0 & 2 & 2 & -1 & -1 & -1 & -1 \\ 0 & 0 & 0 & 1 & 1 & -1 & -1 \end{bmatrix}. \quad (3)$$

The relaxation matrix $\mathbf{S}$, which is a diagonal matrix, can be expressed as

$$\mathbf{S} = \mathrm{diag}[s_0, \ s_1, \ s_2, \ s_3, \ s_4, \ s_5, \ s_6]. \quad (4)$$

Among the relaxation parameters in the diagonal relaxation matrix, the values of s_0, s_1, s_2, and s_3 are set as $s_0 = 1$ and $s_{1,2,3} = 1/\tau$, respectively, where τ is the relaxation time, and the other relaxation parameters, which can be adjusted to achieve a better performance in the calculation, are variables in a range of $0 < s_{4,5,6} < 2$.

The EDF can be expressed as

$$g_i^{\mathrm{eq}} = \begin{cases} w_0\psi & i = 0 \\ w_i\psi\left[1 + \mathbf{e}_i \cdot \mathbf{u}/c_s^2\right] & i \neq 0 \end{cases}. \tag{5}$$

The weight coefficient is given as

$$w_i = \begin{cases} 1/4 & i = 0 \\ 1/8 & i \neq 0 \end{cases}. \tag{6}$$

The corresponding sound speed is $c_s^2 = c^2/4$. The scalar value and diffusivity coefficient are obtained by Eqs. (7) and (8), respectively:

$$\psi = \sum_i g_i, \tag{7}$$

$$D = (\tau - 0.5)c_s^2\Delta t. \tag{8}$$

By using the Chapman-Enskog expansion, the macroscopic governing equation, Eq. (9), can be recovered:

$$\frac{\partial\psi}{\partial t} + \nabla \cdot (\psi\mathbf{u}) = \nabla \cdot (D\nabla\psi). \tag{9}$$

Note that for the situation with $s_{0,1,2,3,4,5,6} = 1/\tau$, the MRT model degenerates to the standard single-relaxation-time (SRT) LB model. The lattice Boltzmann equation, Eq. (1), can be solved through two steps:

Collision step:

$$\hat{g}_i(\mathbf{x}, t + \Delta t) = g_i(\mathbf{x}, t) - [\mathbf{M}^{-1}\mathbf{S}\mathbf{M}]_{ij}\left[g_j(\mathbf{x}, t) - g_j^{\mathrm{eq}}(\mathbf{x}, t)\right]. \tag{10}$$

Streaming step:

$$g_i(\mathbf{x} + \mathbf{e}_i\Delta t, t + \Delta t) = \hat{g}_i(\mathbf{x}, t + \Delta t), \tag{11}$$

where the symbol $\hat{g}_i$ denotes the distribution function after the collision step.

B. Analysis of the LB models for heat transfer in multiphase systems

By setting $\psi = T$, the above LB equation can recover the governing equation of heat transfer in a single phase:

$$\frac{\partial T}{\partial t} + \nabla \cdot (T\mathbf{u}) = \nabla \cdot (\alpha\nabla T), \tag{12}$$

where α is the thermal diffusivity coefficient. However, the governing equation of heat transfer in multiphase systems with variable thermophysical properties is expressed as

$$\frac{\partial(\rho c_p T)}{\partial t} + \nabla \cdot (\rho c_p T\mathbf{u}) = \nabla \cdot (k\nabla T), \tag{13}$$

where k is the thermal conductivity. It can be seen that when the heat capacity ρc_p is variable in the entire domain, Eq. (12) has additional deviation terms compared with Eq. (13). As introduced in the Introduction, there are four approaches to construct the unified LB models for heat transfer in multiphase systems.

For the methods based on adding additional source terms [8–11], the temperature- or enthalpy-based EDF does not change. The additional source terms are added to offset the derivation terms approximately. Since these methods need extra efforts to calculate the source term, which inevitably introduces extra numerical errors, they are disadvantageous compared with other unified models.

For the method to modify the EDF [15], the original EDF is replaced with

$$g_i^{\mathrm{eq}} = \begin{cases} \rho c_p T - (\rho c_p)_0 T + w_0(\rho c_p)_0 T & i = 0 \\ w_i\rho c_p T\left[(\rho c_p)_0/\rho c_p + \mathbf{e}_i \cdot \mathbf{u}/c_s^2\right] & i \neq 0 \end{cases}, \tag{14}$$

where $(\rho c_p)_0$ is the reference heat capacity, which can be chosen as the minimum heat capacity of the entire area to ensure numerical stability. Note that the original EDF is the discretization of the Maxwell-Boltzmann distribution function, while the modified EDF cannot be obtained from the Maxwell-Boltzmann distribution function directly.

Later, the improved virtual heat capacity correction method [17] showed that the modified EDF corresponds to three modifications of the physical model. The first correction is using virtual heat capacity for the entire area; the second correction is adding a source term to the distribution function g_0; and the third correction is using the real heat capacity for the convection term. Finally, it can obtain the same modified EDF.

Another approach [18] is by adjusting the model parameters to satisfy the interface conditions. The EDF used in the simulation is given as

$$g_i^{\mathrm{eq}} = \begin{cases} (1 - 6\Gamma)T & i = 0 \\ \Gamma T\left(1 + \frac{\mathbf{e}_i \cdot \mathbf{u}}{2\Gamma}\right) & i \neq 0 \end{cases}, \tag{15}$$

where Γ is the weight coefficient of the directions $i \neq 0$; it can also be considered as the probability of scalar T transferring to neighbor nodes. The first adjustment is setting

$$\gamma = \frac{\Gamma_B}{\Gamma_A} = \frac{(\rho c_p)_A}{(\rho c_p)_B}, \tag{16}$$

where Γ_A and Γ_B are Γ in phase A and phase B, respectively, and the values are determined by $\max(\Gamma_A, \Gamma_B) = 1/8$. It means that the probability of scalar T transferring from phase A to B (Γ_A) is different from that transferring from phase B to A, i.e., (Γ_B). The second adjustment is revising the streaming process between the two phases as

$$g_i^B(\mathbf{x} + \mathbf{e}_i\Delta t, t + \Delta t) = \gamma\hat{g}_i^A(\mathbf{x}, t), \tag{17}$$

$$g_i^A(\mathbf{x} + \mathbf{e}_i\Delta t, t + \Delta t) = (1/\gamma)\hat{g}_i^B(\mathbf{x}, t). \tag{18}$$

It means that the scalar T is not conserved, i.e., the distribution function in phase A, $\hat{g}_i^A(\mathbf{x}, t)$, changes to $\gamma\hat{g}_i^A(\mathbf{x}, t)$ in phase B. In fact, the second adjustment corresponds to multiply the distribution function with ρc_p. By replacing g_i with $g_i^* = \rho c_p g_i$, the revised streaming process between the two phases, Eqs. (17) and (18), can be recovered to the standard streaming process as follows:

$$g_i^{*B}(\mathbf{x} + \mathbf{e}_i\Delta t, t + \Delta t) = \hat{g}_i^{*A}(\mathbf{x}, t), \tag{19}$$

$$g_i^{*A}(\mathbf{x} + \mathbf{e}_i\Delta t, t + \Delta t) = \hat{g}_i^{*B}(\mathbf{x}, t). \tag{20}$$

Correspondingly, the EDF is modified to

$$g_i^{\mathrm{eq}} = \begin{cases} (1-6\Gamma)\rho c_p T & i=0 \\ \Gamma \rho c_p T\left(1+\frac{\mathbf{e}_i\cdot\mathbf{u}}{2\Gamma}\right) & i\neq 0 \end{cases}. \tag{21}$$

According to the confinement $\max(\Gamma_A,\Gamma_B)=1/8$ and Eq. (16), the values of Γ in different phases can be expressed as a unified scheme as follows:

$$\Gamma = \frac{1}{8}\frac{(\rho c_p)_0}{\rho c_p}. \tag{22}$$

Substituting Eq. (22) into Eq. (21), the final EDF can be expressed as

$$g_i^{\mathrm{eq}} = \begin{cases} \rho c_p T - \frac{3}{4}(\rho c_p)_0 T & i=0 \\ \frac{1}{8}\rho c_p T\left(\frac{(\rho c_p)_0}{\rho c_p}+4\frac{\mathbf{e}_i\cdot\mathbf{u}}{c^2}\right) & i\neq 0 \end{cases}, \tag{23}$$

which is the same as the modified EDF, Eq. (14).

C. Analysis of the LB models for mass transfer in multiphase systems

By setting $\psi = C$ in Eq. (9), we can get the governing equation of mass transfer in a single phase:

$$\frac{\partial C}{\partial t} + \nabla\cdot(C\mathbf{u}) = \nabla\cdot(D\nabla C). \tag{24}$$

According to the analysis in Ref. [21], it is more reasonable to set ϕC as the driving potential of mass transfer, where ϕ is a dimensionless parameter that proportional to the average diffusion velocity of solute molecules. The values of ϕ in the gas and liquid phases are determined by $\phi_G = 1/\max(1,H_e)$ and $\phi_L = H_e/\max(1,H_e)$, where H_e is the distribution coefficient determined by the properties of solute and solutions. The revised Fick's law is given as [21]

$$\mathbf{q}_m = \frac{D}{\phi}\nabla(\phi C). \tag{25}$$

Therefore, the corresponding governing equation for mass transfer in multiphase systems can be written as

$$\frac{\partial C}{\partial t} + \nabla\cdot(C\mathbf{u}) = \nabla\cdot\left[\frac{D}{\phi}\nabla(\phi C)\right]. \tag{26}$$

In the LB model based on modifying the EDF, the modified EDF is given as

$$g_i^{\mathrm{eq}} = \begin{cases} (1-\phi)C + w_0 C\phi & i=0 \\ w_i C\left(\phi+\frac{\mathbf{e}_i\cdot\mathbf{u}}{c_s^2}\right) & i\neq 0 \end{cases}. \tag{27}$$

Through the Chapman-Enskog expansion [21], the governing equation, Eq. (26), can be recovered.

In the LB model based on adjusting the model parameters to satisfy the interface conditions [19], the EDF used in the simulation is given as

$$g_i^{\mathrm{eq}} = \begin{cases} (1-6\Gamma)C & i=0 \\ \Gamma C\left(1+\frac{\mathbf{e}_i\cdot\mathbf{u}}{2\Gamma c^2}\right) & i\neq 0 \end{cases}. \tag{28}$$

The adjustment is setting

$$\frac{\Gamma_G}{\Gamma_L} = \frac{1}{H_e}, \tag{29}$$

where the values of Γ_G and Γ_L are determined by $\max(\Gamma_G,\Gamma_L)=1/8$. It means that the probability of scalar C transferring from liquid to gas (Γ_L) is different from that transferring from gas to liquid, i.e., (Γ_G). The detailed discussion of the physical meaning of Eq. (29) can be seen in Ref. [19].

According to the values of ϕ and Eq. (29), the values of Γ in different phases can be expressed as a unified scheme as follows:

$$\Gamma = \tfrac{1}{8}\phi. \tag{30}$$

Substituting Eq. (30) into Eq. (28), the final EDF can be expressed as

$$g_i^{\mathrm{eq}} = \begin{cases} \left(1-\frac{3}{4}\phi\right)C & i=0 \\ \frac{1}{8}\phi C + \frac{\mathbf{e}_i\cdot\mathbf{u}}{2c^2}C & i\neq 0 \end{cases}. \tag{31}$$

It can be seen that Eq. (31) is equivalent to Eqs. (27), which means that the two LB models based on different perspectives are equivalent.

In addition, it is noted that in the governing equation Eq. (26), the driving potential ϕC can be considered as an introduced continuous scalar. Therefore, the CD problem with a discontinuous scalar value needs to be transformed to the one with a continuous scalar value in LBM.

D. Analysis of the LB models for solid-liquid phase change

The governing equation of heat transfer in a system with solid-liquid phase change can be written as [32]

$$\frac{\partial H}{\partial t} = \frac{\partial(\rho c_p T + \rho f_L L_a)}{\partial t} = -\nabla\cdot(\rho c_p T\mathbf{u}) + \nabla\cdot(k\nabla T), \tag{32}$$

where H, f_L, and L_a are the total enthalpy, fluid fraction, and latent heat, respectively. As introduced in the Introduction, the latent heat source term $\frac{\partial(\rho L_a f_L)}{\partial t}$ is implicit, which significantly increases the computation costs since the implicit latent heat has to be updated through iteration. By adding the latent enthalpy $\rho L_a f_L$ into the total enthalpy term H, the implicit latent enthalpy term can be eliminated. The EDF of the LB model for solid-liquid phase change can be expressed as [32]

$$g_i^{\mathrm{eq}}(\mathbf{x},t) = \begin{cases} \rho H - (\rho c_p)_0 T + w_i(\rho c_p)_0 T & i=0 \\ w_i(\rho c_p)_0 T + w_i \rho c_p T\frac{\mathbf{e}_i\cdot\mathbf{u}}{c_s^2} & i\neq 0 \end{cases}, \tag{33}$$

where $(\rho c_p)_0$ is the reference heat capacity, which is chosen as the minimum heat capacity of the entire area. Here the higher-order terms of the EDF in Ref. [32] are neglected. The modified EDF corresponds to three modifications of the physical model as well.

Owing to the discontinuous heat flux at the phase interface, unphysical numerical diffusion exists [32] for the standard SRT LB model. The two references [32,34] showed that the unphysical numerical diffusion induced by a discontinuous heat flux can be eliminated by adjusting the relaxation parameters in the relaxation matrix. However, the mathematical analyses in the two references were not complete enough, since only the one-dimensional one-phase melting problem was theoretically analyzed. The later research [35] proved that the OTRT model can eliminate the unphysical numerical diffusion of an arbitrary DmQn LB models for both one-phase

and two-phase melting problems. In fact, it can be proven that the OTRT model is equivalent to the MRT model with the adjusted relaxation parameters. Therefore, the MRT model with adjusted relaxation parameters can be proven to have the same performance with the OTRT model in eliminating the unphysical numerical diffusion for both one-phase and two-phase multidimensional melting problems.

As an example, in the D3Q7 MRT model with adjusted relaxation parameters [34], the free relaxation parameters can be set as

$$s_4 = s_5 = s_6 = 2 - 1/\tau. \tag{34}$$

Thus the matrix $\mathbf{M}^{-1}\mathbf{S}\mathbf{M}$ in evolution function Eq. (1) can be expressed as

$$\mathbf{M}^{-1}\mathbf{S}\mathbf{M} = \begin{bmatrix} \frac{6}{7\tau}-\frac{6}{7} & \frac{1}{7}-\frac{1}{7\tau} & \frac{1}{7}-\frac{1}{7\tau} & \frac{1}{7}-\frac{1}{7\tau} & \frac{1}{7}-\frac{1}{7\tau} & \frac{1}{7}-\frac{1}{7\tau} & \frac{1}{7}-\frac{1}{7\tau} \\ \frac{1}{7}-\frac{1}{7\tau} & \frac{1}{7}-\frac{1}{7\tau} & \frac{6}{7\tau}-\frac{6}{7} & \frac{1}{7}-\frac{1}{7\tau} & \frac{1}{7}-\frac{1}{7\tau} & \frac{1}{7}-\frac{1}{7\tau} & \frac{1}{7}-\frac{1}{7\tau} \\ \frac{1}{7}-\frac{1}{7\tau} & \frac{6}{7\tau}-\frac{6}{7} & \frac{1}{7}-\frac{1}{7\tau} & \frac{1}{7}-\frac{1}{7\tau} & \frac{1}{7}-\frac{1}{7\tau} & \frac{1}{7}-\frac{1}{7\tau} & \frac{1}{7}-\frac{1}{7\tau} \\ \frac{1}{7}-\frac{1}{7\tau} & \frac{1}{7}-\frac{1}{7\tau} & \frac{1}{7}-\frac{1}{7\tau} & \frac{1}{7}-\frac{1}{7\tau} & \frac{6}{7\tau}-\frac{6}{7} & \frac{1}{7}-\frac{1}{7\tau} & \frac{1}{7}-\frac{1}{7\tau} \\ \frac{1}{7}-\frac{1}{7\tau} & \frac{1}{7}-\frac{1}{7\tau} & \frac{1}{7}-\frac{1}{7\tau} & \frac{6}{7\tau}-\frac{6}{7} & \frac{1}{7}-\frac{1}{7\tau} & \frac{1}{7}-\frac{1}{7\tau} & \frac{1}{7}-\frac{1}{7\tau} \\ \frac{1}{7}-\frac{1}{7\tau} & \frac{1}{7}-\frac{1}{7\tau} & \frac{1}{7}-\frac{1}{7\tau} & \frac{1}{7}-\frac{1}{7\tau} & \frac{1}{7}-\frac{1}{7\tau} & \frac{6}{7\tau}-\frac{6}{7} & \frac{1}{7}-\frac{1}{7\tau} \\ \frac{1}{7}-\frac{1}{7\tau} & \frac{1}{7}-\frac{1}{7\tau} & \frac{1}{7}-\frac{1}{7\tau} & \frac{1}{7}-\frac{1}{7\tau} & \frac{1}{7}-\frac{1}{7\tau} & \frac{1}{7}-\frac{1}{7\tau} & \frac{6}{7\tau}-\frac{6}{7} \end{bmatrix}. \tag{35}$$

In the LB model we have

$$\sum_i g_i(\mathbf{x},t) - \sum_i g_i^{\mathrm{eq}}(\mathbf{x},t) = 0. \tag{36}$$

Therefore, the matrix $\mathbf{M}^{-1}\mathbf{S}\mathbf{M}$ in Eq. (1) can be replaced by

$$\begin{bmatrix} \frac{1}{\tau}-1 & 0 & 0 & 0 & 0 & 0 & 0 \\ 0 & 0 & \frac{1}{\tau}-1 & 0 & 0 & 0 & 0 \\ 0 & \frac{1}{\tau}-1 & 0 & 0 & 0 & 0 & 0 \\ 0 & 0 & 0 & 0 & \frac{1}{\tau}-1 & 0 & 0 \\ 0 & 0 & 0 & \frac{1}{\tau}-1 & 0 & 0 & 0 \\ 0 & 0 & 0 & 0 & 0 & 0 & \frac{1}{\tau}-1 \\ 0 & 0 & 0 & 0 & 0 & \frac{1}{\tau}-1 & 0 \end{bmatrix}. \tag{37}$$

It can be found that the evolution of distribution function g_i is only related to g_i^{eq}, $g_{\tilde{i}}$, and $g_{\tilde{i}}^{\mathrm{eq}}$, where $\tilde{i}$ denotes the opposite direction of i. The evolution equation, Eq. (1), can be simplified as

$$g_i(\mathbf{x}+\mathbf{e}_i\Delta t, t+\Delta t) = g_i^{\mathrm{eq}}(\mathbf{x},t) - (1-1/\tau)\left[g_{\tilde{i}}(\mathbf{x},t) - g_{\tilde{i}}^{\mathrm{eq}}(\mathbf{x},t)\right]. \tag{38}$$

For the OTRT model, the evolution equation can be given as

$$\begin{aligned} g_i(\mathbf{x}+\mathbf{e}_i\Delta t, t+\Delta t) &= g_i^{\mathrm{eq}}(\mathbf{x},t) + \left(1-\frac{1}{2\tau_s}-\frac{1}{2\tau_a}\right)\left[g_i(\mathbf{x},t) - g_i^{\mathrm{eq}}(\mathbf{x},t)\right] \\ &\quad - \left(\frac{1}{2\tau_s}-\frac{1}{2\tau_a}\right)\left[g_{\tilde{i}}(\mathbf{x},t) - g_{\tilde{i}}^{\mathrm{eq}}(\mathbf{x},t)\right], \end{aligned} \tag{39}$$

where τ_a and τ_s are the antisymmetric and symmetric relaxation times, respectively, and their values are determined by

$$\tau_a = \tau, \quad 1/\tau_a + 1/\tau_s = 2. \tag{40}$$

By substituting Eq. (40) into Eq. (39), Eq. (39) can be simplified to Eq. (38), which means that the MRT model for solid-liquid phase change with adjusted relaxation parameters is equivalent to the OTRT model mathematically.

III. THE COMPREHENSIVE LB MODEL FOR DIFFERENT CD PROBLEMS IN MULTIPHASE SYSTEMS

A. Introduction of the CMLBM

According to the analyses above, the treatments for different kinds of CD problems in unified LB models can be concluded. For the CD problems with a continuous scalar value and a continuous flux, no special treatment is needed. For the CD problems with a discontinuous scalar value and a continuous flux, a continuous scalar can be introduced to transform the problem to the one with both continuous scalar value and flux. For the CD problems with a continuous scalar value and a discontinuous flux, the MRT LB model with an optimal relation between the relaxation parameters or the simplified model given by Eq. (38) is needed. Based on the unified LB model for CD problems with a continuous scalar value and a discontinuous flux, the CMLBM that can deal with the three kinds of CD problems in multiphase systems can be constructed.

The governing equations of the CD problems in multiphase systems can be written in a unified scheme as

$$\frac{\partial A(\psi)}{\partial t} + \nabla\cdot[B(\psi)\mathbf{u}] = \nabla\cdot[D\nabla C(\psi)], \tag{41}$$

where $A(\psi)$, $B(\psi)$, and $C(\psi)$ are the functions of the scalar ψ. The corresponding EDF of the LB model can be

given as

$$g_i^{\mathrm{eq}} = \begin{cases} A(\psi) - C(\psi) + w_0 C(\psi) & i = 0 \\ w_i C(\psi) + w_i B(\psi)\frac{\mathbf{e}_i \cdot \mathbf{u}}{c_s^2} & i \neq 0 \end{cases}. \tag{42}$$

The corresponding equilibrium moment space $\mathbf{m}$ is

$$\mathbf{m}^{eq} = \mathbf{M}\mathbf{g}^{eq} = [A(\psi), u_x B(\psi), u_y B(\psi), u_z B(\psi), 6A(\psi) - 21C(\psi)/4, 0, 0]. \tag{43}$$

The evolution function and relaxation matrix $\mathbf{M}$ are given as Eq. (1) and Eq. (4), respectively. The relaxation parameters in the relaxation matrix are given as $s_0 = 1$, $s_{1,2,3} = 1/\tau$, and $s_{4,5,6} = 2 - 1/\tau$.

The macroscopic parameters $A(\psi)$ and D are determined by

$$A(\psi) = \sum_i g_i, \tag{44}$$

$$D = (\tau - 0.5)c_s^2 \Delta t. \tag{45}$$

By using the Chapman-Enskog expansion (see Appendix), the macroscopic governing equation, Eq. (41), can be recovered.

In addition, considering that some CD problems are anisotropic, the above LB model is extended to the anisotropic situation by replacing the relaxation matrix by [42]

$$\mathbf{S} = \begin{bmatrix} s_0 & 0 & 0 & 0 & 0 & 0 & 0 \\ 0 & s_{xx} & s_{xy} & s_{xz} & 0 & 0 & 0 \\ 0 & s_{yx} & s_{yy} & s_{yz} & 0 & 0 & 0 \\ 0 & s_{zx} & s_{zy} & s_{zz} & 0 & 0 & 0 \\ 0 & 0 & 0 & 0 & s_4 & 0 & 0 \\ 0 & 0 & 0 & 0 & 0 & s_5 & 0 \\ 0 & 0 & 0 & 0 & 0 & 0 & s_6 \end{bmatrix}. \tag{46}$$

The relaxation parameters $s_{ij}(i, j = x, y, z)$ are determined by

$$\mathbf{D} = \tfrac{1}{4}\Delta t(\mathbf{I} - \mathbf{A}/2)\mathbf{A}^{-1}, \tag{47}$$

where $\mathbf{D}$ is the diffusivity coefficient matrix and $\mathbf{A} = s_{ij}$. The other relaxation parameters are given as $s_0 = 1$, $s_4 = s_5 = s_6 = 2 - s_{xx}$.

By using Chapman-Enskog expansion (see Appendix), the LB model can recover the anisotropic governing equation:

$$\frac{\partial A(\psi)}{\partial t} + \nabla \cdot [B(\psi)\mathbf{u}] = \nabla \cdot [\mathbf{D}\nabla C(\psi)]. \tag{48}$$

It is underlined that for the isotropic CD problems in multiphase systems, the simplified evolution equation (38) is recommended. The simplified CMLBM is labeled by SCMLBM. It is equivalent to the MRT model in both accuracy and stability while it has a similar low computation cost with the standard SRT model.

B. Boundary treatments

For the Dirichlet boundary condition, the simplified boundary scheme in Ref. [43] is adopted, which can be expressed as

$$g_i(\mathbf{x}_b, t + \Delta t) = -g_{\tilde{i}}(\mathbf{x}_b, t + \Delta t) + 2w_i C(\psi), \tag{49}$$

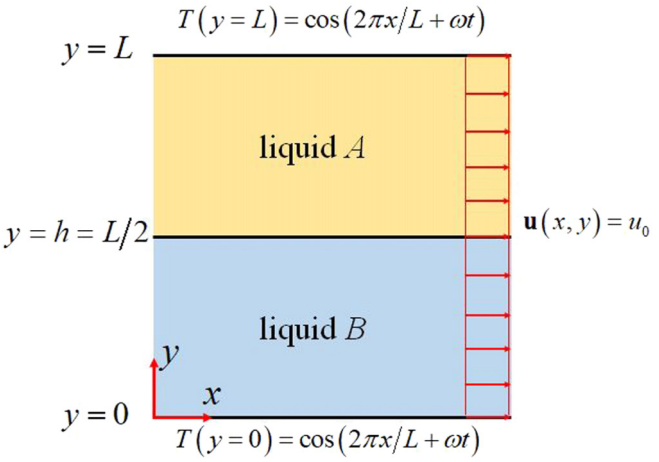

FIG. 1. Schematic of heat transfer in a channel filled with two fluids.

where $\mathbf{x}_b$ is the boundary point, $\tilde{i}$ denotes the opposite direction of i, and $C(\psi)$ is the scalar value at the boundary point.

For the Neumann boundary condition with zero flux, the Neumann boundary scheme in Ref. [42] is adopted:

$$g_i(\mathbf{x}_b, t + \Delta t) = \hat{g}_{\tilde{i}}(\mathbf{x}_b, t + \Delta t). \tag{50}$$

IV. RESULTS AND DISCUSSION

A. The unsteady heat convection diffusion in a channel filled with two fluids

As an example of CD problems with both continuous scalar value and flux, an unsteady heat convection-diffusion problem in a channel filled with two fluids is considered. The functions $A(\psi)$, $B(\psi)$, and $C(\psi)$ in the SCMLBM correspond to $\rho c_p T$, $\rho c_p T$, and $(\rho c_p)_0 T$, respectively. The macroscopic parameters including the temperature T and thermal conductivity k are determined by

$$T = \sum_i g_i/(\rho c_p), \tag{51}$$

$$\frac{k}{(\rho c_p)_0} = (\tau - 0.5)c_s^2 \Delta t. \tag{52}$$

As shown in Fig. 1, the computational domain of size $L \times L$ is filled with liquid A in the upper area and liquid B in the lower area. The entire domain has a uniform horizontal velocity u_0. The upper and lower boundaries are set as a Dirichlet condition:

$$T(y = 0, L) = \cos(\beta x + \omega t), \tag{53}$$

where $\beta = 2\pi/L$, ω is the frequency. The left and right boundaries are periodic. In the numerical simulation, the two periodic boundaries are set as Dirichlet condition as well, and the temperature distributions at the two boundaries are determined by the analytical solution. The analytical solution of the problem is given as

$$T(x, y, t) = \begin{cases} \mathrm{Re}\{e^{i(\beta x + \omega t)}[\gamma_1 e^{-\lambda_1 y} + (1 - \gamma_1)e^{\lambda_1 y}]\} & y \leqslant h \\ \mathrm{Re}\{e^{i(\beta x + \omega t)}[\gamma_2 e^{-\lambda_2 y} + (1 - \gamma_2 e^{-\lambda_2 L})e^{-\lambda_2 (L - y)}]\} & y > h \end{cases}, \tag{54}$$

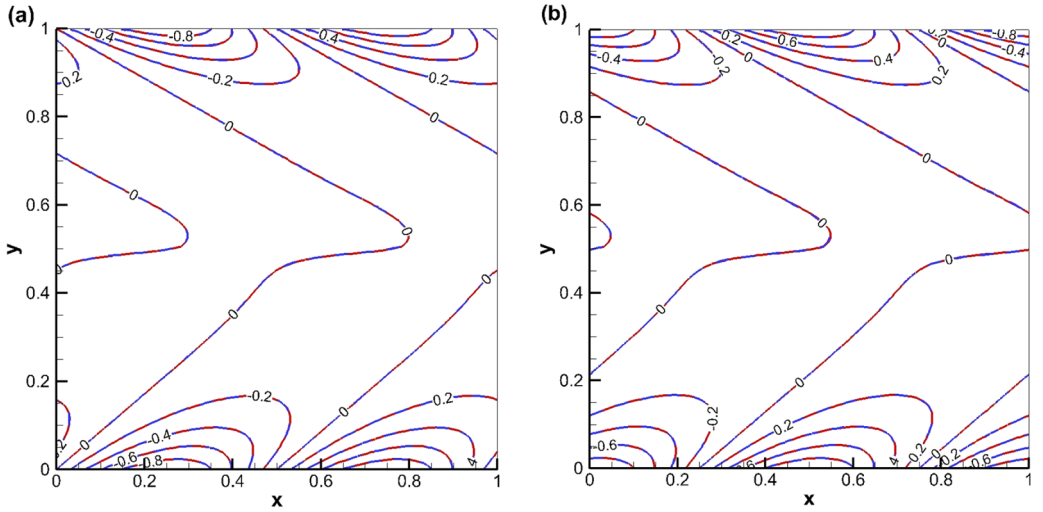

FIG. 2. Comparisons of temperature contours at Fourier numbers $F = 0.025$ (a) and $F = 0.05$ (b) between the calculated results (blue dashed line) and analytical solutions (red solid line).

where the function Re denotes the real part of a complex number. The parameters in the analytical solution are calculated by

$$\lambda_1 = \beta\sqrt{1 + i\frac{\omega + u_0\beta}{\alpha_B\beta^2}}, \quad \lambda_2 = \beta\sqrt{1 + i\frac{\omega + u_0\beta}{\alpha_A\beta^2}}, \tag{55a}$$

$$a_1 = e^{-\lambda_1 h}, \quad a_2 = e^{-\lambda_2 h}, \quad a_3 = e^{-\lambda_2 L}, \tag{55b}$$

$$\gamma_1 = \frac{\lambda_1\left(a_3^2 - a_2^2\right) + R_\alpha R_{\rho c_p}\lambda_2\left(2a_1a_2a_3 - a_2^2 - a_3^2\right)}{\left(\lambda_1 + R_\alpha R_{\rho c_p}\lambda_2\right)\left(a_1^2a_3^2 - a_2^2\right) - \left(\lambda_1 - R_\alpha R_{\rho c_p}\lambda_2\right)\left(a_1^2a_2^2 - a_3^2\right)}, \tag{55c}$$

$$\gamma_2 = \frac{\lambda_1\left(a_1^2a_3 + a_3 - 2a_1a_2\right) + R_\alpha R_{\rho c_p}\lambda_2 a_3\left(a_1^2 - 1\right)}{\left(\lambda_1 + R_\alpha R_{\rho c_p}\lambda_2\right)\left(a_1^2a_3^2 - a_2^2\right) - \left(\lambda_1 - R_\alpha R_{\rho c_p}\lambda_2\right)\left(a_1^2a_2^2 - a_3^2\right)}, \tag{55d}$$

where R_α and $R_{\rho c_p}$ are the ratio of diffusivity coefficient defined as $R_\alpha = \alpha_A/\alpha_B$ and the ratio of heat capacity defined as $R_{\rho c_p} = (\rho c_p)_A/(\rho c_p)_B$, respectively.

The parameters of the problem are given as $L = 1$, $R_\alpha = 0.5$, $R_{\rho c_p} = 10$, $u_0 = 10D_A/L$, $\omega = 20\pi D_A/L^2$. First, the grid number used for simulation is 100×100, and the relaxation times in liquid A and liquid B are set as 0.9 and 2.5, respectively.

To validate the SCMLBM, the temperature contours at two different Fourier numbers $F = tD_A/L^2 = 0.025$ and 0.05 are captured and then compared with the corresponding analytical solutions. As shown in Fig. 2, the calculated temperature

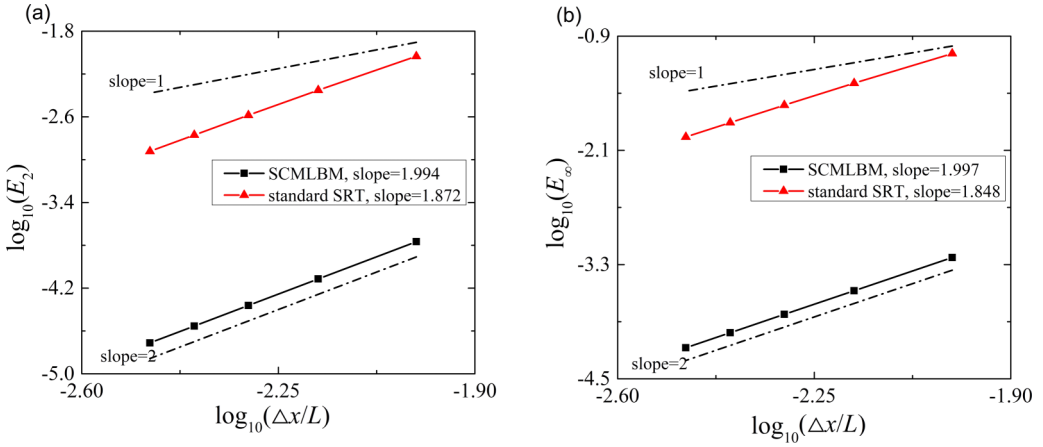

FIG. 3. Numerical error E_2 (a) and E_∞ (b) analyses of the SCMLBM and the standard SRT LB model for unsteady heat convection diffusion in a channel filled with two fluids.

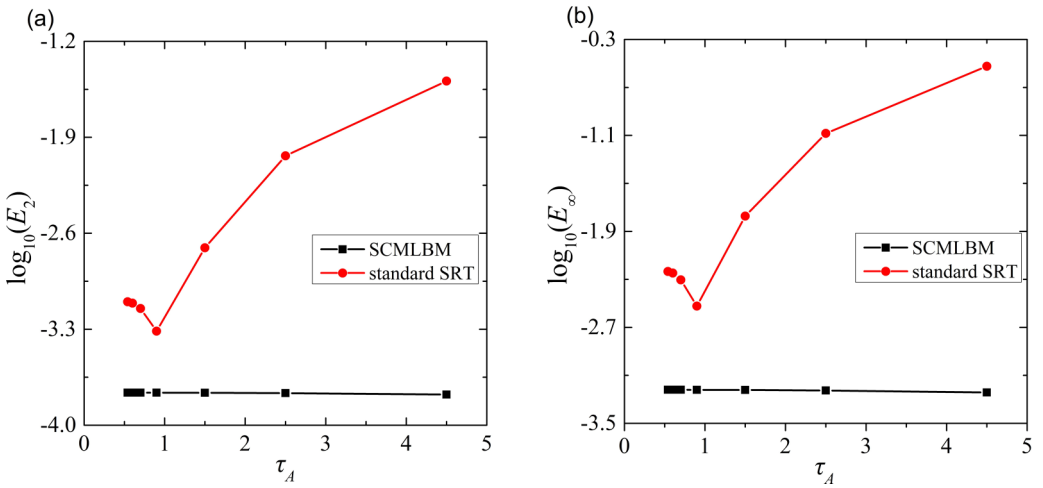

FIG. 4. Numerical errors E_2 (a) and E_∞ (b) of the SCMLBM and the standard SRT LB model for heat convection diffusion in a multiphase system at different relaxation times.

fields at the two transient moments show good agreement with the analytical solutions.

To compare the convergence orders of the SCMLBM and the standard SRT LB model, the mesh dependence test is performed for the two LB models. The average error E_2 and the maximum error E_∞ of the two LB models at different mesh sizes are shown in Fig. 3. The average error E_2 and maximum error E_∞ are respectively defined by

$$E_2 = \sqrt{\frac{1}{N}\sum (T - T_a)^2}, \tag{56}$$

$E_\infty = \max\{|T - T_a|\}$, where N is the total number of the grid points, and T_a is the analytical solution. The numerical errors are evaluated at $F = 0.025$.

As shown in Fig. 3(a), the convergence order based on E_2 of the SCMLBM is 1.994, which is slightly higher than the standard SRT LB model with a convergence order of 1.872. The result is consistent with the second-order accuracy shown in Chapman-Enskog expansion. In addition, the average error of the SCMLBM is much less than the standard SRT model. As to the maximum error E_∞, Fig. 3(b) shows that the SCMLBM has a slightly higher convergence order and a much smaller maximum error than the standard SRT model as well.

To analyze the numerical errors further, the relations between the numerical errors and the relaxation time are investigated. Here the relaxation time in phase A (τ_A) is set as a variable. As shown in Fig. 4, with the relaxation time increasing, the E_2 and E_∞ of the standard SRT model show large variation, while those of the SCMLBM have no obvious variation. In a large range of τ_A, the numerical errors of the SCMLBM are significantly smaller than the standard SRT model.

In conclusion, the results indicate that the SCMLBM has better accuracy than the standard SRT LB model for the heat CD problem in multiphase systems.

B. Transient mass transfer between two liquid films

This case considers the transient mass transfer between two liquid films. The functions $A(\psi)$, $B(\psi)$, and $C(\psi)$ in the SCMLBM correspond to C, C, and ϕC, respectively. The macroscopic parameters including the concentration C and diffusivity coefficient D are determined by

$$C = \sum_i g_i, \tag{57}$$

$$\frac{D}{\phi} = (\tau - 0.5)c_s^2 \Delta t. \tag{58}$$

As shown in Fig. 5, the computational area is filled with fluid A in the lower half and fluid B in the upper half. The dynamic viscosity ratio between the two fluids is set as $\mu_A/\mu_B = 4$. The upper wall is fixed at a constant velocity u_0 while the lower wall is stationary. Thus, the stationary velocity field can be given as

$$u = \begin{cases} 1.6u_0 y/L & -L/2 \leqslant y \leqslant 0 \\ 0.8u_0 + 0.4u_0(y - L/2)/L & 0 < y \leqslant L/2 \end{cases}. \tag{59}$$

It is set as an input in the simulation.

The other parameters are given as $D_B = 0.1$, $D_A = 0.025$, $H_e = C_A/C_B = 2$, $u_0 = 16D_A/L$. The initial concentration

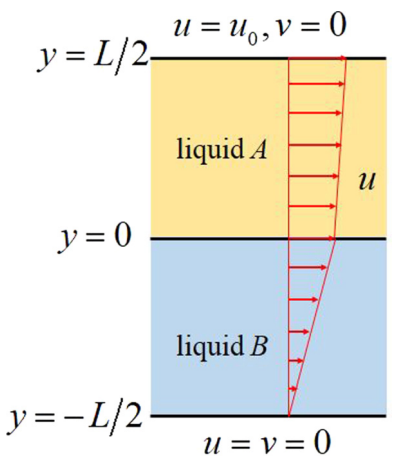

FIG. 5. Schematic of the two-fluid flow between two liquid films.

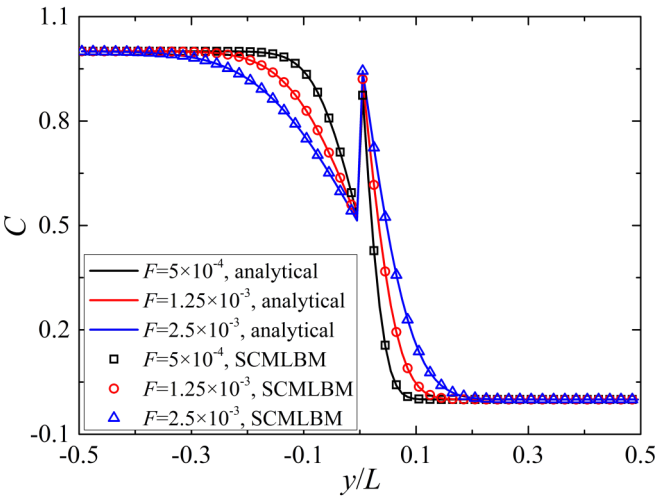

FIG. 6. Concentration distributions at different transient moments.

distribution is set as

$$C = \begin{cases} C_B = 1 & y \leqslant 0 \\ C_A = 0 & y > 0 \end{cases}. \tag{60}$$

The left and right boundaries are periodic. Therefore, the problem can be simplified to one dimensional. The simulation time is limited to be short enough in the range $F = tD_A/L^2 \leqslant 2.5 \times 10^{-3}$; thus the area can be considered as infinite in the vertical direction approximately. The transient concentration distributions at $F = 5 \times 10^{-4}$, 1.25×10^{-3}, and 2.5×10^{-3} are outputted and then compared with the corresponding analytical solutions. The analytical solution for the problem in an infinite system can be given as

$$C = \begin{cases} C_B + (C_A - H_e C_B)\frac{1+\mathrm{erf}(y/\sqrt{4D_B t})}{H_e+\sqrt{D_B/D_A}} & y \leqslant 0 \\ C_A + (C_B - C_A/H_e)\frac{1-\mathrm{erf}(y/\sqrt{4D_A t})}{1/H_e+\sqrt{D_A/D_B}} & y > 0 \end{cases}. \tag{61}$$

As shown in Fig. 6, the concentration has an obvious jump at the interface. However, the calculated results are always in good agreement with the analytical solutions at different transient moments.

To compare the convergence order of the SCMLBM with the standard SRT model, the mesh dependence test is performed for the two models. The relaxation times in phase A and phase B are fixed at 0.7 and 0.9, respectively. The numerical errors E_2 and E_∞ at different mesh sizes are shown in Fig. 7, where the numerical errors are calculated at $F = 5 \times 10^{-4}$. The results show that the two LB models have a similar convergence order near 2 and the errors of SCMLBM are always smaller than the standard SRT model at different mesh sizes.

In addition, the relaxation time dependence test is made to compare the two models. The numerical errors E_2 and E_∞ at different relaxation times of the two LB models are investigated. Figure 8 shows the variations of E_2 and E_∞ with τ_A increasing, where τ_A is the relaxation time in phase A. It can be seen that the numerical errors E_2 and E_∞ of the SCMLBM are generally smaller than those of the standard SRT LB model in a large τ_A range. Only for τ_A near 0.9, the numerical errors E_2 and E_∞ of the SCMLBM are slightly larger than the standard SRT LB model. Combining the results of mesh dependence test, it can be concluded that the SCMLBM has better numerical accuracy than the standard SRT model in general for the mass transfer problem in multiphase systems.

In addition, the more detailed simulations of mass transfer in multiphase systems with convection and large concentration jump and diffusivity ratio can be seen in Ref. [19]. The model in this reference is based on the MRT model proposed by Li *et al.* [34], which is proven to be equivalent to the SCMLBM according to the analysis in Sec. II. D.

C. Solid-liquid phase change

As an example of the CD problem in a multiphase system with a continuous scalar value and a discontinuous flux, the solid-liquid phase change problems are considered in this section. The functions $A(\psi)$, $B(\psi)$, and $C(\psi)$ in the SCMLBM correspond to ρH, $\rho c_p T$, and $(\rho c_p)_0 T$, respectively. The macroscopic parameters including the total enthalpy H, liquid

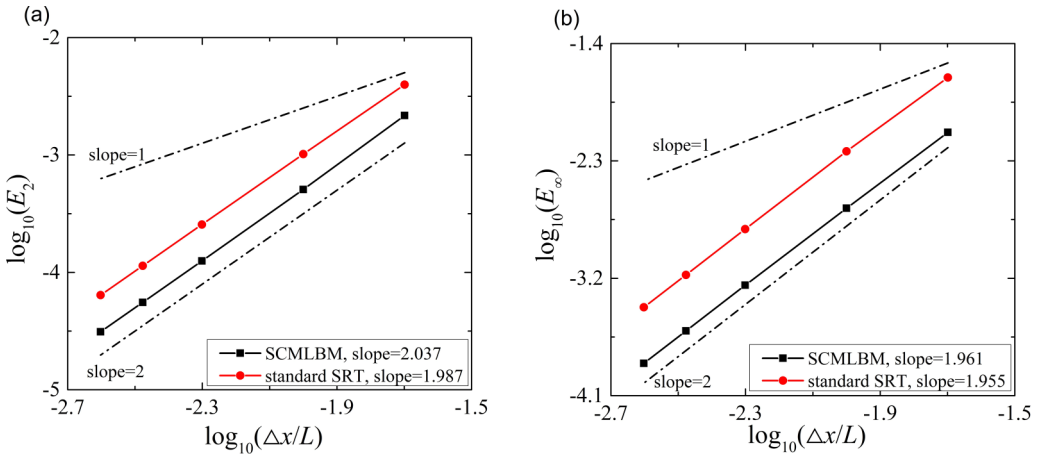

FIG. 7. Numerical errors E_2 (a) and E_∞ (b) of the SCMLBM and the standard SRT LB model for mass transfer in a multiphase system at different mesh sizes.

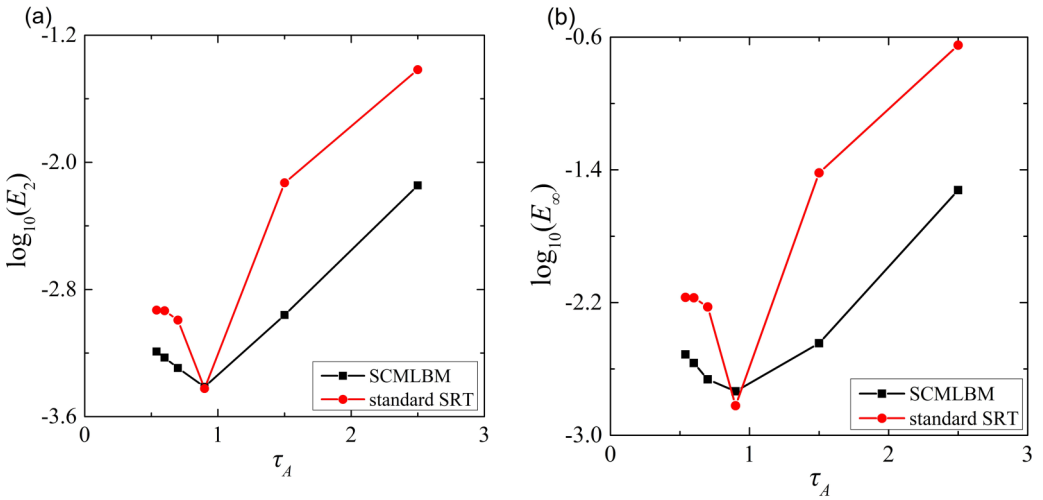

FIG. 8. Numerical errors E_2 (a) and E_∞ (b) of the SCMLBM and the standard SRT LB model for mass transfer in a multiphase system at different relaxation times.

fraction f_L, temperature T, and thermal conductivity k are determined by

$$H = \sum_i g_i/\rho, \tag{62}$$

$$f_L = \begin{cases} 0 & H \leqslant H_s \\ \frac{H-H_s}{H_l-H_s} & H_s < H < H_l \\ 1 & H \geqslant H_l \end{cases}, \tag{63}$$

$$T = \begin{cases} T_s - \frac{H_s-H}{c_{p,s}} & H \leqslant H_s \\ \frac{H_l-H}{H_l-H_s}T_s + \frac{H-H_s}{H_l-H_s}T_l & H_s < H < H_l \\ T_l - \frac{H-H_l}{c_{p,l}} & H \geqslant H_l \end{cases}, \tag{64}$$

$$\frac{k}{(\rho c_p)_0} = (\tau - 0.5)c_s^2 \Delta t, \tag{65}$$

where $H_s = c_{p,s}T_s$ is the total enthalpy at the solidus temperature T_s, and $H_l = c_{p,s}T_s + L_a$ is the total enthalpy at the liquidus temperature T_l.

The physical model shown in Fig. 9 is a one-dimensional infinite system. At the initial time, it is filled with the solid phase at temperature T_0. The left wall is kept at a constant high temperature T_h, which is higher than the melting temperature T_m, then the solid phase starts melting.

First, the one-phase melting, which means that the initial temperature T_0 equals the melting temperature T_m and the solid phase is inactive, is considered. The analytical solution

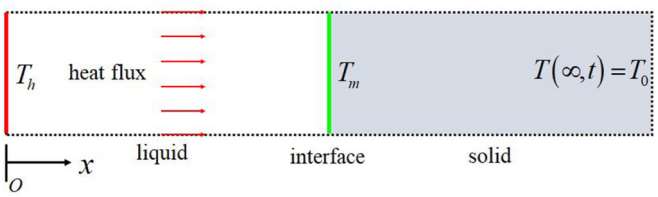

FIG. 9. The physical model of the solid-liquid phase change.

of this case is given by [32]

$$T(x,t) = \begin{cases} T_h - \frac{T_h-T_m}{\mathrm{erf}(\chi)}\mathrm{erf}\left(\frac{x}{2\sqrt{k_l/\rho c_{p,l}t}}\right), & 0 \leqslant x \leqslant X_i(t) \\ T_m, & x > X_i(t) \end{cases}, \tag{66}$$

where $X_i(t) = 2\chi\sqrt{k_l/(\rho c_{p,l})}$ is the location of the phase interface, and χ is the root of the following equation:

$$\frac{S_l}{\exp(\chi^2)\mathrm{erf}(\chi)} = \chi\sqrt{\pi}, \tag{67}$$

where the Stefan number S_l is defined as $S_l = c_{p,l}(T_h - T_m)/L$, and the subscripts l and s denote the parameters in the liquid phase and solid phase, respectively.

The parameters used in the simulation are set as follows: $T_h = 1$, $T_m = T_0 = 0$, $\rho_l = \rho_s = 1$, $S_l = 0.01$, $c_{p,l} = 1$, $k_l = 1/6$, $R_{\rho c_p} = (\rho_s c_{p,s})/(\rho_l c_{p,l}) = 1$, and $R_k = k_s/k_l = 1$. The relaxation times in the liquid phase and solid phase are both set as 1.5. Owing to the inactive solid phase, the thermophysical property differences between the two phases are not considered.

The temperature and liquid fraction distributions at three transient moments $t = 10$, 50, and 100 calculated by the SCMLBM are captured and compared with the corresponding analytical solutions. As shown in Fig. 10, the calculated results at different transient moments agree well with the analytical solutions. In addition, all the phase interfaces are exactly one lattice spacing, and the temperatures of the solid phase are exactly at T_m, which means that there is no unphysical numerical diffusion induced by the discontinuous heat flux.

Second, the two-phase melting, which means that the initial temperature T_0 is lower than the melting temperature T_m and the solid phase is active, is considered. The analytical solution of the temperature distribution is given as [32]

$$T(x,t) = \begin{cases} T_h - \frac{T_h-T_m}{\mathrm{erf}(\chi)}\mathrm{erf}\left(\frac{x}{2\sqrt{k_l/\rho_l c_{p,l}t}}\right), & 0 \leqslant x \leqslant X_i(t) \\ T_0 + \frac{T_m-T_0}{\mathrm{erf}(\chi/\sqrt{R_\alpha})}\mathrm{erfc}\left(\frac{x}{2\sqrt{k_s/\rho_s c_{p,s}t}}\right), & x > X_i(t) \end{cases}, \tag{68}$$

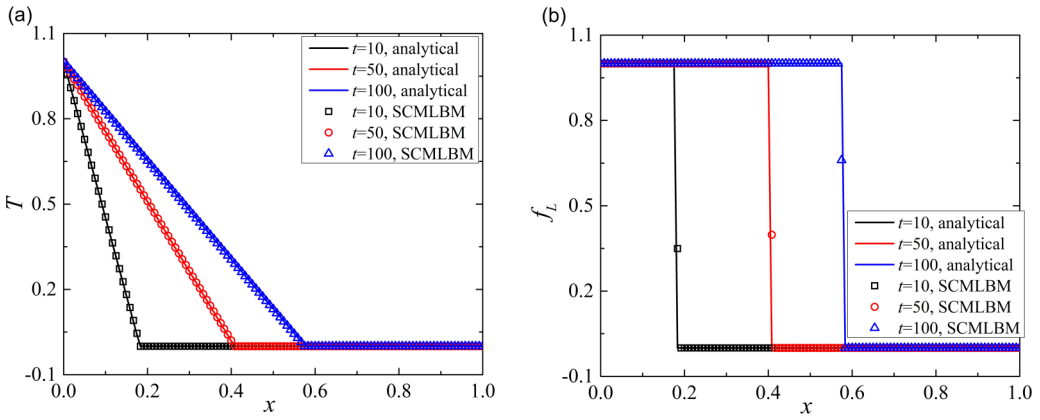

FIG. 10. Comparisons of T (a) and f_L (b) between the calculated results and the analytical solutions at different times for one-dimensional one-phase melting by conduction.

where $R_\alpha = [k_s/(\rho_s c_{p,s})]/[k_l/(\rho_l c_{p,l})]$ is the ratio of thermal diffusivities of the solid and the liquid phases, $X_i(t) = 2\chi\sqrt{k_l/(\rho c_{p,l})}$ is the location of the phase interface, and χ is the root of the following equation:

$$\frac{S_l}{\exp(\chi^2)\mathrm{erf}(\chi)} - \frac{S_s\sqrt{R_\alpha}}{\exp(\chi^2/\sqrt{R_\alpha})\mathrm{erfc}(\chi/\sqrt{R_\alpha})} = \chi\sqrt{\pi}, \tag{69}$$

where $S_l = c_{p,l}(T_h - T_m)/L$ and $S_s = c_{p,s}(T_m - T_0)/L$.

In the present simulation, the parameters are set as follows: $T_h = 1$, $T_m = 0.5$, $T_0 = 0$, $\rho_l = \rho_s = 1$, $c_{p,l} = 1$, $k_l = 1/6$, $R_{c_p} = c_{p,s}/c_{p,l} = 4$, $R_k = k_s/k_l = 2$, $S_l = 0.005$, $S_s = 0.02$. The relaxation times in the liquid phase and solid phase are set as 1.5 and 2.5, respectively.

For validation, the temperature and liquid fraction distributions at three transient moments $t = 5$, 20, and 50 calculated by the SCMLBM are captured and then compared with the corresponding analytical solutions. As shown in Fig. 11, the calculated results always show good agreement with the analytical solutions. In addition, the phase interface widths at different transient moments are always one lattice spacing, which means that there is no unphysical numerical diffusion induced by the discontinuous heat flux.

In conclusion, the SCMLBM can effectively eliminate the unphysical numerical diffusion of both one-phase and two-phase solid-liquid melting problems, which is consistent with the theoretical analysis [35]. Note that according to the theoretical analysis in Sec. II. D, the SCMLBM for solid-liquid phase change is equivalent to the OTRT LB model for solid-liquid phase change [35]. More simulations of two-dimensional and three-dimensional solid-liquid phase change with convection by using OTRT LB model can be found in Ref. [35]. The results indicate that the SCMLBM can also effectively eliminate the unphysical numerical diffusion of two-dimensional and three-dimensional situations.

D. Heat conduction in a two-layer composite anisotropic medium

Since some heat conductive materials are anisotropic, heat conduction in a two-layer composite anisotropic medium is considered in this section. The functions $A(\psi)$, $B(\psi)$, and $C(\psi)$ in the CMLBM correspond to $\rho c_p T$, $\rho c_p T$, and $(\rho c_p)_0 T$, respectively. The temperature T is obtained through Eq. (51) as well and the thermal conductivity matrix $\mathbf{k}$ are determined by

$$\frac{\mathbf{k}}{(\rho c_p)_0} = \frac{1}{4}\Delta t(\mathbf{I} - \mathbf{A}/2)\mathbf{A}^{-1}. \tag{70}$$

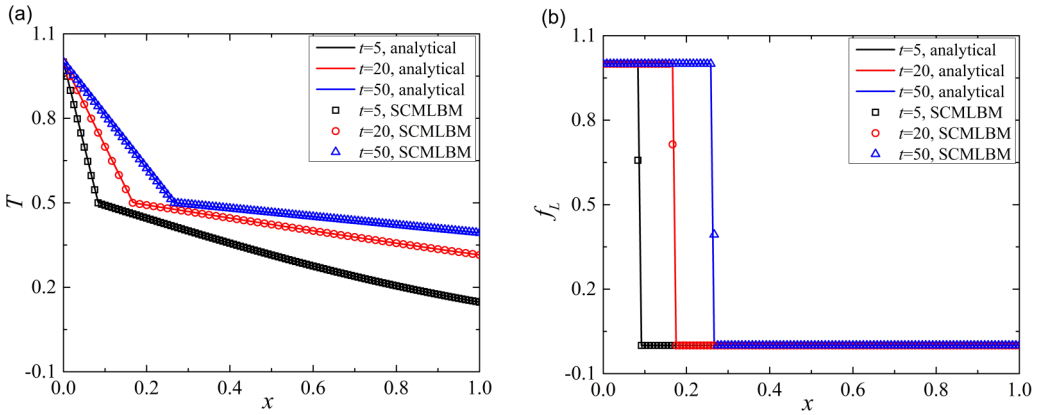

FIG. 11. Comparisons of T (a) and f_L (b) between the calculated results and the analytical solutions at different moments for one-dimensional two-phase melting by conduction.

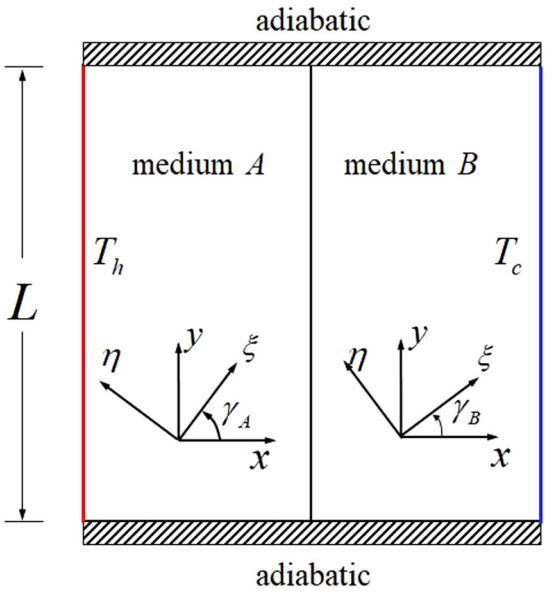

FIG. 12. The physical model of the composite anisotropic medium.

As shown in Fig. 12, the physical model is a square composite medium that consists of medium A in the left half and medium B in the right half. The size is $L \times L$ and $L = 1$. The upper and lower boundaries are adiabatic, and the left and right boundaries are imposed with constant high temperature T_h and constant low temperature T_c, respectively. The anisotropy angles of the media A and B are set as $\gamma_A = 45^\circ$ and $\gamma_B = -45^\circ$. Here the anisotropy angle is defined as the angle from the horizontal direction x to the first principal direction ξ. The thermal conductivity matrixes $\begin{bmatrix} k_{xx} & k_{xy} \\ k_{yx} & k_{yy} \end{bmatrix}$ of the media A and B are given as $\begin{bmatrix} 0.6 & 0.4 \\ 0.4 & 0.6 \end{bmatrix}$ and $\begin{bmatrix} 0.15 & -0.05 \\ -0.05 & 0.15 \end{bmatrix}$, respectively, the heat capacities of the media A and B are given as $(\rho c_p)_A = 10$ and $(\rho c_p)_B = 100$, respectively. To validate the present model, the dimensionless temperature $\theta = (T - T_c)/(T_h - T_c)$ contours at the transient time $F = t(k_{xx})_A/[L^2(\rho c_p)_A] = 1$ and steady state are compared with those calculated by the finite volume method (FVM) using software Fluent. The uniform mesh of size 100×100 is used for both methods.

As shown in Fig. 13, the dimensionless temperature contours given by FVM show obvious discontinuity at the phase

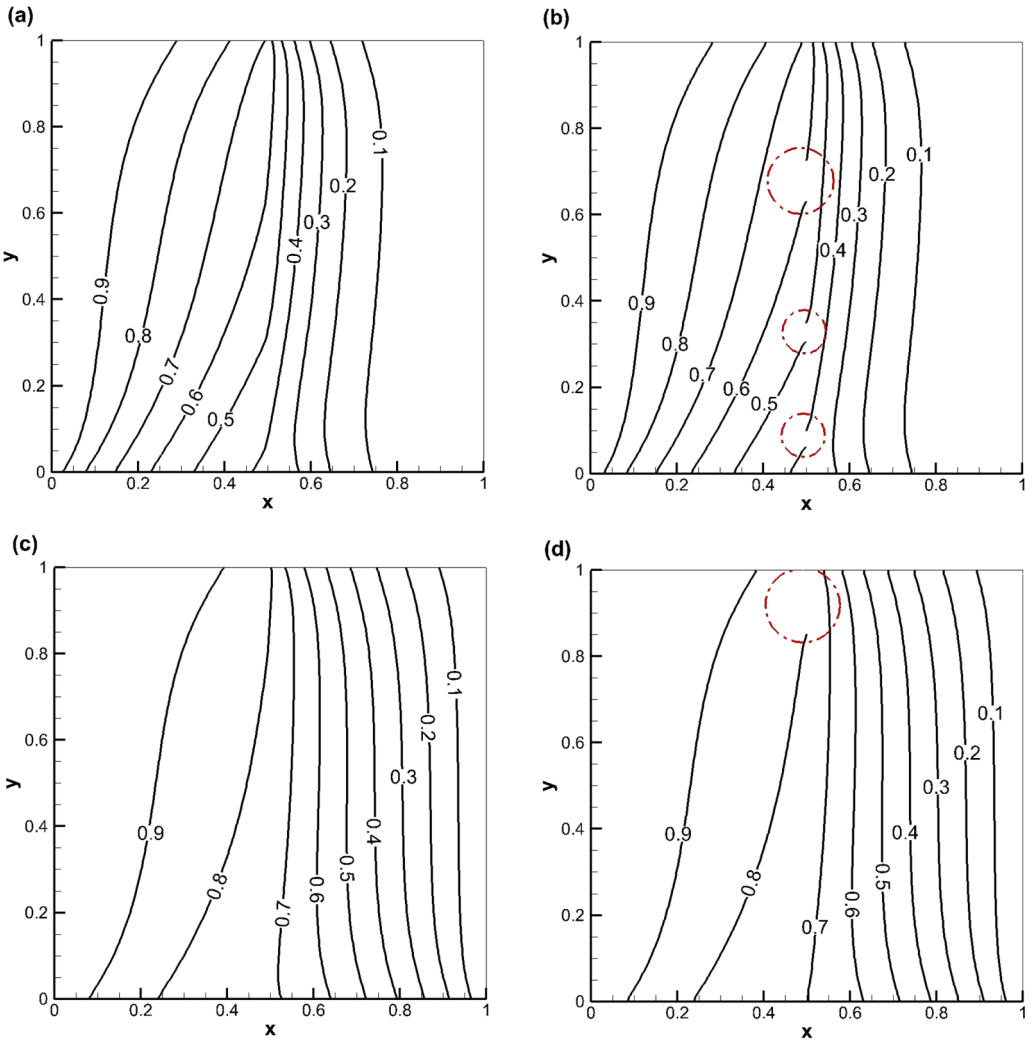

FIG. 13. Temperature contours at Fourier number $F = 1$ and steady state calculated by the CMLBM and FVM: (a) $F = 1$, CMLBM, (b) $F = 1$, FVM, (c) steady, CMLBM and (d) steady, FVM; the area in the solid red circles is the discontinuous contour lines.

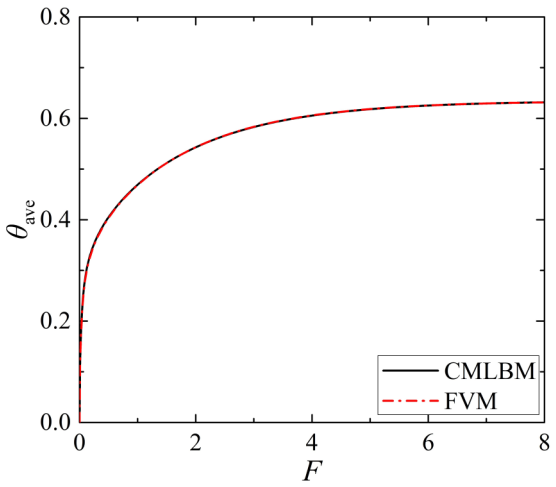

FIG. 14. Comparison of the transient average dimensionless temperature between the CMLBM and FVM.

interface. However, the CMLBM can ensure the temperature continuity at the phase interface without any additional treatment. In addition, the contours calculated by the CMLBM match well with those given by FVM at both the transient and steady states.

Furthermore, to make comparison quantitatively, the transient average dimensionless temperature θ_{ave} of the entire area is shown in Fig. 14. It can be seen that the curves of θ_{ave} obtained by the two methods show good agreement. The two comparisons indicate that the CMLBM is able to simulate anisotropic heat transfer in multiphase systems. In addition, the temperature continuity at the phase interface can be well ensured by using CMLBM.

V. CONCLUSION

In the present paper, the typical unified LB models for the CD problems in multiphase systems are analyzed. As a summary, the CD problems in multiphase systems can be classified into three groups: CD problems with both continuous scalar value and flux, a discontinuous scalar value and a continuous flux, and a continuous scalar value and a discontinuous flux. Detailed analyses are performed to show the equivalence between the unified LB models for the three kinds of CD problems. In addition, the treatments for the three kinds of CD problems in LB models are concluded. For the CD problems with a continuous scalar value and a continuous flux, no special treatment is needed. For the CD problems with a discontinuous scalar value and a continuous flux, a new defined continuous scalar needs to be introduced to transform the problem to the one with both continuous scalar value and flux. For the CD problems with a continuous scalar value and a discontinuous flux, the MRT LB model with an optimal relation between the relaxation parameters or the simplified model given in Eq. (38) is needed.

As a consequence, considering different kinds of isotropic and anisotropic CD problems in multiphase systems, the CMLBM is proposed. For the isotropic situations, the simplified CMLBM, i.e., SCMLBM, is given. It is equivalent to the standard SRT model in simplicity; however, it has the same accuracy and stability with the MRT LB model with an optimal relation between the relaxation parameters. Four typical CD problems in multiphase systems are calculated to validate the CMLBM. For the isotropic heat and mass transfer problems in multiphase systems with continuous fluxes, the CMLBM has better numerical accuracy than the standard SRT model in general. For the isotropic solid-liquid melting problem with a discontinuous flux, it can effectively eliminate the unphysical numerical diffusion. For the anisotropic heat transfer problem in multiphase systems, it can ensure the temperature continuity at the phase interface well while the FVM cannot. These results show that the CMLBM is a competitive LB model for dealing with different CD problems in multiphase systems.

ACKNOWLEDGMENTS

This work is financially supported by the National Natural Science Foundation of China (Grants No. 41574176 and No. 41672234). In addition, the financial support from the China Scholarship Council to the first author is gratefully acknowledged.

APPENDIX: CHAPMAN-ENSKOG EXPANSION TO RECOVER THE GOVERNING EQUATION OF ANISOTROPIC HEAT TRANSFER IN MULTIPHASE SYSTEMS

By using the Taylor expansion, Eq. (1) can be written as

$$\mathbf{Dg}+\frac{\Delta t}{2}\mathbf{D}^2\mathbf{g}+O(\Delta t^2)=-\frac{\mathbf{M}^{-1}\mathbf{SM}}{\Delta t}(\mathbf{g}-\mathbf{g}^{\mathrm{eq}}), \tag{A1}$$

where $\mathbf{D}=\mathrm{diag}(D_0,D_1,\ldots,D_6)$, and $D_i=\partial_t+\mathbf{e}_i\cdot\nabla$. In the moment space, Eq. (A1) is written as

$$\mathbf{MDM}^{-1}\mathbf{m}+\frac{\Delta t}{2}(\mathbf{MDM}^{-1})^2\mathbf{m}+O(\Delta t^2) =-\frac{\mathbf{S}}{\Delta t}(\mathbf{m}-\mathbf{m}^{\mathrm{eq}}). \tag{A2}$$

Then we expand $\mathbf{m}$ as

$$\mathbf{m}=\mathbf{m}^{(0)}+\varepsilon\mathbf{m}^{(1)}+\varepsilon^2\mathbf{m}^{(2)}+O(\varepsilon^3), \tag{A3}$$

where ε is a small parameter. To derive the macroscopic governing equation, two macroscopic timescales $t_1=\varepsilon t$, $t_2=\varepsilon^2 t$ and a macroscopic length scale $x_1=\varepsilon x$ are introduced to recover the control equation, and thus we have

$$\partial_t=\varepsilon\partial_{t_1}+\varepsilon^2\partial_{t_2},\quad \nabla=\nabla_1. \tag{A4}$$

The matrix $\mathbf{MDM}^{-1}$ can be written as

$$\mathbf{MDM}^{-1}=\mathbf{I}\partial_t+\mathbf{E}\cdot\nabla=\mathbf{I}\left(\varepsilon\partial_{t_1}+\varepsilon^2\partial_{t_2}\right)+\varepsilon\mathbf{E}\cdot\nabla_1, \tag{A5}$$

where $\mathbf{I}$ is the unit matrix, $\mathbf{E}=(\mathbf{E}_x,\mathbf{E}_y,\mathbf{E}_z)$ and

$$\mathbf{E}_x=\mathbf{M}\mathrm{diag}[\mathbf{e}_{0x},\ \mathbf{e}_{1x},\ldots,\mathbf{e}_{6x}]\mathbf{M}^{-1}, \tag{A6a}$$

$$\mathbf{E}_y=\mathbf{M}\mathrm{diag}[\mathbf{e}_{0y},\ \mathbf{e}_{1y},\ldots,\mathbf{e}_{6y}]\mathbf{M}^{-1}, \tag{A6b}$$

$$\mathbf{E}_z=\mathbf{M}\mathrm{diag}[\mathbf{e}_{0z},\ \mathbf{e}_{1z},\ldots,\mathbf{e}_{6z}]\mathbf{M}^{-1}. \tag{A6c}$$

Substituting the expansions Eqs. (A3) and (A5) in Eq. (A2), we can rewrite Eq. (A2) in the different orders of the parameter ε as

$$\varepsilon^0 : \mathbf{m}^{(0)} = \mathbf{m}^{\mathrm{eq}}, \tag{A7a}$$

$$\varepsilon^1 : \left(\mathbf{I}\partial_{t_1} + \mathbf{E}\cdot\nabla_1\right)\mathbf{m}^{(0)} = \frac{\mathbf{S}}{\Delta t}\mathbf{m}^{(1)}, \tag{A7b}$$

$$\varepsilon^2 : \partial_{t_2}\mathbf{m}^{(0)} + \left(\mathbf{I}\partial_{t_1} + \mathbf{E}\cdot\nabla_1\right)\left(\mathbf{I} - \frac{1}{2}\mathbf{S}\right)\mathbf{m}^{(1)} = \frac{\mathbf{S}}{\Delta t}\mathbf{m}^{(2)}. \tag{A7c}$$

For the CD problems, only the conserved moment m_0 in Eqs. (A7a), (A7b) and (A7c) is needed. The corresponding equations can be given as

$$\varepsilon^0 : m_0^{(0)} = m_0^{\mathrm{eq}}, \tag{A8a}$$

$$\varepsilon^1 : \partial_{t_1} m_0^{(0)} + \partial_{x_1} m_1^{(0)} + \partial_{y_1} m_2^{(0)} + \partial_{z_1} m_3^{(0)} = -\frac{s_0}{\Delta t} m_0^{(1)}, \tag{A8b}$$

$$\varepsilon^2 : \partial_{t_2} m_0^{(0)} + \partial_{t_1}\left[\left(1 - \frac{s_0}{2}\right)m_0^{(1)}\right] + \nabla_1 \cdot \left[\left(\mathbf{I} - \frac{1}{2}\mathbf{A}\right)\begin{pmatrix} m_1^{(1)} \\ m_2^{(1)} \\ m_3^{(1)} \end{pmatrix}\right] = -\frac{s_0}{\Delta t} m_0^{(2)}. \tag{A8c}$$

Owing to $m_0 = m_0^{(0)} = m_0^{\mathrm{eq}}$, we can obtain

$$m_0^{(n)} = 0 (n \geqslant 1). \tag{A9}$$

Thus, Eq. (A8b) and Eq. (A8c) can be simplified as

$$\varepsilon^1 : \partial_{t_1} m_0^{(0)} + \partial_{x_1} m_1^{(0)} + \partial_{y_1} m_2^{(0)} + \partial_{z_1} m_3^{(0)} = 0. \tag{A10a}$$

$$\varepsilon^2 : \partial_{t_2} m_0^{(0)} + \nabla_1 \cdot \left[\left(\mathbf{I} - \frac{1}{2}\mathbf{A}\right)\begin{pmatrix} m_1^{(1)} \\ m_2^{(1)} \\ m_3^{(1)} \end{pmatrix}\right] = 0. \tag{A10b}$$

Combining the equations in Eq. (A7b), we can obtain the following equation:

$$\begin{aligned} -\frac{\mathbf{A}}{\Delta t}\begin{pmatrix} m_1^{(1)} \\ m_2^{(1)} \\ m_3^{(1)} \end{pmatrix} &= \begin{bmatrix} \partial_{t_1} m_1^{(0)} + \partial_{x_1}\left(\frac{2}{7} m_0^{(0)} - \frac{1}{21} m_4^{(0)} + \frac{1}{3} m_5^{(0)}\right) \\ \partial_{t_1} m_2^{(0)} + \partial_{y_1}\left(\frac{2}{7} m_0^{(0)} - \frac{1}{21} m_4^{(0)} - \frac{1}{6} m_5^{(0)} - \frac{1}{2} m_6^{(0)}\right) \\ \partial_{t_1} m_3^{(0)} + \partial_{z_1}\left(\frac{2}{7} m_0^{(0)} - \frac{1}{21} m_4^{(0)} - \frac{1}{6} m_5^{(0)} - \frac{1}{2} m_6^{(0)}\right) \end{bmatrix} \\ &= \partial_{t_1}[B(\psi)\mathbf{u}] + \frac{1}{4}\nabla_1 C(\psi). \end{aligned} \tag{A11}$$

Substituting Eq. (A11) into Eq. (A10b) yields

$$\partial_{t_2}(A(\psi)) = \nabla_1 \cdot \left\{\Delta t\left(\mathbf{I} - \tfrac{1}{2}\mathbf{A}\right)\mathbf{A}^{-1}\left[\partial_{t_1}(B(\psi)\mathbf{u}) + \tfrac{1}{4}\nabla_1 C(\psi)\right]\right\}. \tag{A12}$$

Combining Eqs. (A10a) and (A12) and neglecting the higher-order term $\nabla_1 \cdot [\Delta t(\mathbf{I} - \frac{1}{2}\mathbf{A})\mathbf{A}^{-1}\partial_{t_1}(B(\psi)\mathbf{u})]$, we can get the final governing equation,

$$\partial_t A(\psi) + \nabla \cdot [B(\psi)\mathbf{u}] = \nabla \cdot [\mathbf{D}\nabla C(\psi)], \tag{A13}$$

where the diffusivity coefficient matrix $\mathbf{D}$ is determined by

$$\mathbf{D} = \tfrac{1}{4}\Delta t\left(\mathbf{I} - \tfrac{1}{2}\mathbf{A}\right)\mathbf{A}^{-1}. \tag{A14}$$

[1] M. Mozafari-Shamsi, M. Sefid, and G. Imani, Numer. Heat Transf. B **70**, 559 (2016).

[2] L. Li, C. Chen, R. Mei, and J. F. Klausner, Phys. Rev. E **89**, 043308 (2014).

[3] M. Seddiq, M. Maerefat, and M. Mirzaei, Int. J. Therm. Sci. **75**, 28 (2014).

[4] J. H. Lu, H. Y. Lei, and C. S. Dai, Int. J. Heat Mass Transf. **114**, 268 (2017).

[5] A. A. Mohamad, Q. W. Tao, Y. L. He, and S. Bawazeer, Numer. Heat Transf. B **67**, 124 (2015).

[6] G. Imani, M. Maerefat, and K. Hooman, Numer. Heat Transf. A **62**, 798 (2012).

[7] F. Meng, M. Wang, and Z. Li, Int. J. Heat Fluid Flow **29**, 1203 (2008).
[8] S. Chen, Y. Y. Yan, and W. Gong, Int. J. Heat Mass Transf. **107**, 862 (2017).
[9] H. Rihab, N. Moudhaffar, B. N. Sassi, and P. Patrick, Int. J. Heat Mass Transf. **100**, 728 (2016).
[10] Y. Hu, D. Li, S. Shu, and X. Niu, Phys. Rev. E **92**, 063305 (2015).
[11] H. Karani and C. Huber, Phys. Rev. E **91**, 023304 (2015).
[12] W. Wu, S. L. Zhang, S. F. Wang, and K. Ling, Numer. Heat Transf. B **72**, 130 (2017).
[13] S. Chen, Int. J. Therm. Sci. **124**, 477 (2018).
[14] D. Gao, Z. Chen, L. Chen, and D. Zhang, Int. J. Heat Mass Transf. **105**, 673 (2017).
[15] S. Chen, B. Yang, and C. Zheng, Int. J. Heat Mass Transf. **102**, 637 (2016).
[16] J. H. Lu, H. Y. Lei, and C. S. Dai, Int. J. Heat Mass Transf. **126**, 1275 (2018).
[17] J. H. Lu, H. Y. Lei, and C. S. Dai, Int. J. Therm. Sci. **116**, 22 (2017).
[18] H. Yoshida, T. Kobayashi, H. Hayashi, T. Kinjo, H. Washizu, and K. Fukuzawa, Phys. Rev. E **90**, 013303 (2014).
[19] J. H. Lu, H. Y. Lei, and C. S. Dai, Chem. Eng. Sci. **199**, 319 (2019).
[20] G. R. Molaeimanesh and M. H. Akbari, Int. J. Hydrogen Energy **40**, 5169 (2015).
[21] J. H. Lu, H. Y. Lei, and C. S. Dai, Int. J. Heat Mass Transf. **132**, 519 (2019).
[22] D. Chatterjee, Numer. Heat Transf. B **58**, 55 (2010).
[23] W. Zhu, M. Wang, and H. Chen, Int. J. Therm. Sci. **117**, 239 (2017).
[24] D. Chatterjee and S. Chakraborty, Phys. Lett. A **341**, 320 (2005).
[25] D. Chatterjee and S. Chakraborty, Int. J. Therm. Sci. **47**, 552 (2008).
[26] R. Huang and H. Wu, J. Comput. Phys. **277**, 305 (2014).
[27] M. Eshraghi and S. D. Felicelli, Int. J. Heat Mass Tran. **55**, 2420 (2012).
[28] W. S. Jiaung, J. R. Ho, and C. P. Kuo, Numer. Heat Transf. B **2**, 167 (2001).
[29] C. Hubera, A. Parmigianib, B. Chopardb, M. Mangac, and O. Bachmannd, Int. J. Heat Fluid Flow **29**, 1469 (2008).
[30] A. Ali Rabienataj Darzi, M. Farhadi, M. Jourabian, and Y. Vazifeshenas, Int. J. Numer. Methods Heat Fluid Flow **24**, 221 (2013).
[31] R. Huang, H. Wu, and P. Cheng, Int. J. Heat Mass Transf. **59**, 295 (2013).
[32] R. Huang and H. Wu, J. Comput. Phys. **294**, 346 (2015).
[33] Y. Hu, D. Li, S. Shu, and X. Niu, Int. J. Heat Mass Transf. **113**, 1168 (2017).
[34] D. Li, Z. X. Tong, Q. Ren, Y. L. He, and W. Q. Tao, Int. J. Heat Mass Transf. **115**, 1334 (2017).
[35] J. H. Lu, H. Y. Lei, and C. S. Dai, Int. J. Therm. Sci. **135**, 17 (2019).
[36] Y. T. Mu, Z. L. Gu, P. He, and W. Q. Tao, Phys. Rev. E **98**, 043309 (2018).
[37] K. Guo, L. Li, G. Xiao, N. AuYeung, and R. Mei, Int. J. Heat Mass Transf. **88**, 306 (2015).
[38] J. Huang and W. A. Yong, J. Comput. Phys. **300**, 70 (2015).
[39] Z. Hu, J. Huang, and W. A. Yong, Phys. Rev. E **93**, 043320 (2016).
[40] Z. Chai, B. Shi, and Z. Guo, J. Sci. Comput. **69**, 355 (2016).
[41] B. Shi and Z. Guo, Phys. Rev. E **79**, 016701 (2009).
[42] H. Yoshida and M. Nagaoka, J. Comput. Phys. **229**, 7774 (2010).
[43] L. Li, R. Mei, and J. F. Klausner, J. Comput. Phys. **237**, 366 (2013).